Surface & Coatings Technology 350 (2018) 436–444

Contents lists available at ScienceDirect

Surface & Coatings Technology

journal homepage: www.elsevier.com/locate/surfcoat

Improved hardness and wear resistance of plasma sprayed nanostructured NiCrBSi coating via short-time heat treatment

Liang-Yu Chen[a,b,c], Tianxiang Xu[a], Sheng Lu[a,*], Ze-Xin Wang[a], Shujin Chen[a], Lai-Chang Zhang[c,*]

[a] School of Materials Science and Engineering, Jiangsu University of Science and Technology, Zhenjiang, Jiangsu 212003, China
[b] School of Science, Jiangsu University of Science and Technology, Zhenjiang, Jiangsu 212003, China
[c] School of Engineering, Edith Cowan University, 270 Joondalup Drive, Joondalup, Perth, WA 6027, Australia

ARTICLE INFO

Keywords:
NiCrBSi
Amorphous phase
Precipitate
Hardness
Wear resistance

ABSTRACT

NiCrBSi alloy coatings deposited by atmospheric plasma spray technology were heated at 440 °C, 460 °C, and 480 °C for a short-time respectively to achieve a better understanding of the relationship between their microstructures and properties. Optical microscopy, scanning electron microscopy, X-ray diffraction, transmission electron microscopy and tribological tests were conducted to evaluate the microstructures and wear performance of the coatings. Both the hardness and wear resistance of the coatings increase at the initial stage of short-time heat treatment followed by decreasing. The heat-treated coatings show 15.4% higher maximum hardness and 60% lower minimum wear volume than the as-sprayed one. The as-sprayed NiCrBSi coating possesses a mixed microstructure mainly composed of the crystalline phases and the amorphous phase (about 10 vol%). After 3-min heat treatment at 480 °C, the volume fraction of the amorphous phase decreases to 1.6 vol%, while the fractions of compounds (such as Ni_3B and Cr_3B_4) and γ-Ni increase correspondingly. The precipitates of Ni_3B and Cr_3B_4 are responsible for the hardening of the coatings. As heat treatment proceeds, the γ-Ni grains coarsen, leading to a deceasing tendency in the hardness and wear resistance of the coatings. As the abrasive modes of the coatings are not varied after short-time heat treatment, the hardness of the coatings plays a dominant role in the wear resistance of the coatings.

1. Introduction

Surface engineering plays an important role in minimizing wear-induced damage and corrosion-induced damage in many industries [1–6]. It is well known that atmospheric plasma spray technology (APS) can produce reliable coatings with low-cost and high efficiency from a variety of materials to provide suitable performance [7–13]. Among the coatings, NiCrBSi alloys have been widely used in various industrial fields thanks to their favorable wear and corrosion resistance properties [14–17]. However, the shortcomings like porosity, inhomogeneous and poor bonding between splats in the as-sprayed NiCrBSi coatings by APS make the coatings insufficient properties to meet some severe industrial demands [17].

Many researchers have devoted to further improve the properties of NiCrBSi coatings. Post-heat treatment is known as the one of the useful methods [18–22]. Bergant et al. [18, 19] investigated the effects of post-heat treatment and remelting on the quality of the flame sprayed NiCrBSi coatings and found that heat treatment at 900 °C for 1 h could significantly enhance the hardness and wear resistance of the coatings. Nicolas et al. [20] adopted the combination of APS and in situ laser remelting by diode laser process to modify the structural characteristics of NiCrBSi and NiCrBSi-WC coatings. The results showed that a dendritic structure was induced and the porosities of as-sprayed coatings were decreased, thereby improving the mechanical properties of the coating. Houdková et al. [21] discussed the mechanical properties of NiCrBSi coatings processed by flame remelting, furnace remelting, electric resistance remelting and laser remelting. These four remelting technologies successfully eliminated the splat boundaries, thereby improving the abrasive wear resistance and corrosion resistance properties. Liu et al. [22] prepared the NiCrBSi coatings by hybrid plasma spray/in situ laser remelting process and found that the longitudinal component of the residual stress was the highest. It is noted that most previous studies focused on the effects of the temperatures of post-heat treatments near or above the melting point of NiCrBSi alloy [18–22]. However, the success of applying these methods was significantly restricted on the conditions of the facilities and operators, in addition to the high cost of remelting.

In fact, NiCrBSi is a self-flux alloy and its melting point is about

* Corresponding authors.
E-mail addresses: lusheng_ktz@just.edu.cn (S. Lu), l.zhang@ecu.edu.au, lczhangimr@gmail.com (L.-C. Zhang).

https://doi.org/10.1016/j.surfcoat.2018.07.037
Received 26 March 2018; Received in revised form 9 July 2018; Accepted 10 July 2018
Available online 12 July 2018
0257-8972/

1110 °C, much lower than the temperature of plasma arc (about 3000–12,000 °C depending on distance from the nozzle) [19, 23]. Hence, flight particles become molten or partially molten during deposition. When the particles are deposited on the substrates the amorphous phase is inevitably generated due to the rapid cooling rate [24]. The amorphous phase is always in a metastable state and would crystallize once external energy is high enough to trigger the transformation from amorphous phase to crystalline phases, that is nucleation and growth of the new crystalline phase [25–28]. Many studies [24, 25, 29–31] have reported that the crystallization of the amorphous phase in the NiCrBSi coating takes place during heat treatment at a relative low temperature (such as 400 °C). Considering the transformation of the amorphous phase to crystalline phases, the alteration in microstructure of NiCrBSi coatings would take place during heat treatment, thereby changing the properties of the coatings. Therefore, further understanding of the evolution in the microstructures and resultant properties of NiCrBSi coatings during heat treatment can guide the optimization of processing in order to improve the performance of NiCrBSi coatings.

This work aimed to study the effect of short-time heat treatment on the microstructural evolutions and properties of the atmospheric plasma sprayed NiCrBSi coatings. To make a better understanding of the microstructural evolution in the as-sprayed NiCrBSi coatings during the short-time heat treatment, furnace heat treatments for only several minutes were carried out at 440 °C, 460 °C and 480 °C respectively. As suggested by Li et al. [25], the crystallization of the amorphous phase in NiCrBSi coating took place at 400 °C. Therefore, annealing at the selected temperatures would manipulate the microstructures of the as-sprayed NiCrBSi coatings. Then the microstructures, phase constituents and hardness of the as-sprayed and heat-treated coatings were systematically characterized. The tribological behavior of these coatings was also investigated.

2. Experimental

2.1. Sample preparation and short-time heat treatment

NiCrBSi alloy powder from the North of New Material Science and Technology Co. Ltd. was chosen as the feedstock material. The particle size of the powder ranges between 45 and 109 μm. The 2Cr13 steel was used as substrates with the dimensions of 40 mm × 40 mm × 5 mm. The chemical compositions of the NiCrBSi alloy powder and the substrate are given in Table 1.

Since the roughness of the substrates has a significant influence on the adhesion between the coating and the substrate, before spraying, the substrates were polished to a mirror surface and then blasted by alumina grits for about 15 s to ensure a similar surface roughness among the substrates used in this experiment. The NiCrBSi powder was kept in a holding oven at 200 °C in air for 2 h for drying. The spraying parameters adopted in this work are listed in Table 2. The coatings were air cooled to room temperature at the end of the spraying process. The thicknesses of the as-sprayed NiCrBSi coatings were about 400 μm.

The NiCrBSi alloy was a kind of Ni-based alloy and the Ni content of the NiCrBSi alloy powder in this work was about 70 wt%. The melting point of pure Ni is 1453 °C, hence the recrystallization temperature of Ni (i.e. $0.4T_m$, where T_m is melting point) is about 417 °C in theory. Considering the face-centered cubic (FCC) γ-Ni phase is the primary phase of the NiCrBSi coating [1], the microstructural manipulation of the NiCrBSi coating after heat treatment should take the behavior of the Ni phase into account. Hence, selecting a suitable heat treatment temperature above the recrystallization temperature of Ni is necessary to investigate the effect of the recrystallization of Ni grains on the performance of the NiCrBSi coatings. In this work, the short-time heat treatments were selected at 440 °C, 460 °C and 480 °C (all were higher than the recrystallization temperature of Ni), and were held for 0.5 min, 1.5 min, 3 min, 5 min and 15 min at each temperature, respectively. The heat-treated samples were named after their heat treatment temperature and dwelling time; for example, S440-3 stood for the sample treated at 440 °C for 3 min. All the samples were furnace heat treated. After heat treatment, the samples were air cooled.

Table 1
The chemical compositions of NiCrBSi powder and 2Cr13 steel substrate (in wt %).

Elements	C	Si	B	Cr	Mn	Ti	Fe	Ni
NiCrBSi powder	0.63	4.50	2.97	16.20	–	–	5.31	Bal.
2Cr13 steel substrate	0.16	0.80	–	13.00	0.80	0.20	Bal.	0.60

Table 2
Main parameters of the plasma spraying.

Parameters	Values
Voltage (V)	60
Current (A)	500
Gun traverse rate (mm/s)	30
Main gas Ar (MPa)	55
Feed gas Ar (MPa)	28
Spray distance (mm)	80

2.2. Coating characterizations

The test pieces were mechanically ground with SiC paper up to 2000 grits and then polished to a mirror surface by a diamond paste with a particle size of 1.5 μm. The polished samples were etched by a mixed solution composed of $HCl:HNO_3:H_2O$ = 1:10:10 (in vol%). Optical Microscopy (OM, ZeissAxioskop2-MAT) was used to observe the microstructures of the coatings. The porosities were obtained by OM images of the non-etched coatings. To reduce the influence of random error, the porosities were all randomly selected and measured from ten OM images which were binarized by the software Image J2X. In binary images, the pores would be represented by a single color. Then the porosity was obtained by calculating the percentage of the area of this single color in the binary image in accordance with the ASTM Standard E2109-01 [31]. Furthermore, a high-resolution transmission electron microscopy (TEM, JEM-2100F) with energy dispersive spectrometer (EDS) was used to analyze the microstructures of the coatings. The specimens prepared for TEM characterization were ground to approximate 100 μm thick. Final thinning to electron transparency was accomplished by using a twin jet polisher with a mixed solution composed of $HClO_4:C_4H_9OH:CH_3OH$ = 6:39:55 (in vol%) at a temperature of −30 °C. The phase analysis was carried out by X-ray diffraction (XRD, D8 Advance A25X diffractometer) with a monochromatic Cu K_α source, the scanning range of 30–80°, scanning speed of 2°/min and scanning step of 0.02°. The Jade 6.5 software was used to analyze the XRD data. The integrated areas for each diffraction peak in the XRD patterns were determined by using the peak-fitting program Origin with Pearson VII function [26, 32, 33]. Based on the integrated areas, the volume fraction (V_f) for each phase was calculated in a similar manner to the Ref. [26, 32, 33] using the equation below:

$$V_{f,i} = \frac{A_i}{\Sigma A_i} \quad (1)$$

where $V_{f,\,i}$ is the volume fraction of a phase, A_i is the total integrated area of this phase and ΣA_i is the total integrated area for all phases detected in an XRD pattern.

The Vickers hardness of the coatings was measured by German automatic hardness tester (KB30S). The load for indentation was 5 N on the surface of the coating with the dwell time of 15 s. The reported Vickers hardness of each sample was averaged from ten individual tested points.

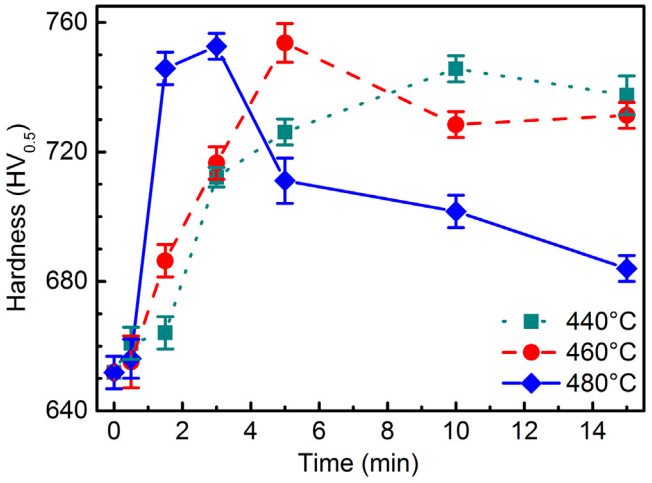

Fig. 1. Variations in hardness of the coatings treated at different temperature.

2.3. Tribological tests

The tribological tests were conducted on a high temperature tribometer (Bruker UMT-2) without lubrication in air. The samples were 10 mm × 10 mm × 5 mm in size with grinding and polishing before test. The pin-on-disc tribological test was realized according to ASTM G99. Testing parameters were as follows: 20 N load; ZrO_2, 5 mm diameter counterpart; 4 mm diameter wear track; 50 rpm slide speed; 1800 s testing time; room temperature. For each sample, three different measurements were performed. The morphologies of the coating samples after tribological tests were observed by scanning electron microscopy (SEM, Merlin Compact). The volumes of the wear tracks were measured by 3D confocal laser-microscopy (Olympus OLS4000) at 5 different places.

3. Results and discussion

3.1. Hardness

The hardness of the 2Cr13 steel substrate is about 269 $HV_{0.5}$. Fig. 1 shows the variations in the hardness of the coatings short-time treated at different temperatures. Obviously, the hardness of the as-sprayed sample (650 $HV_{0.5}$) is much higher than that of the steel substrate. As seen from Fig. 1, the hardness of the coatings tends to rise firstly at the initial stage of heat treatments at all selected temperatures. The highest value of hardness is around 750 $HV_{0.5}$ for all coatings. The higher temperature of the heat treatment, the shorter time to reach the highest value of hardness (e.g. 10 min for 440 °C, 5 min for 460 °C and 3 min for 480 °C). The highest hardness of coatings is about 15.4% higher than that of the as-sprayed sample (650 $HV_{0.5}$). As heat treatment proceeds, the coatings show a decreasing trend in hardness at all selected temperatures. It seems that the short-time heat treatment has a great influence on the hardness of the coatings even though the temperature of heat treatment is significantly lower than the melting point of the NiCrBSi alloy [19].

3.2. Wear performance

At each selected temperature, the coatings with the highest hardness (S440-10, S460-5 and S480-3) and the coatings treated for 15 min were selected for tribological tests to illustrate the wear performance of the coatings during short-time heat treatment. The 2Cr13 steel substrate and the as-sprayed sample were used as a reference. Fig. 2 exhibits the friction coefficients of these samples. The friction coefficient of the as-sprayed sample (0.146) is much lower than that of the 2Cr13 steel substrate (0.207), but substantially greater than those for heat

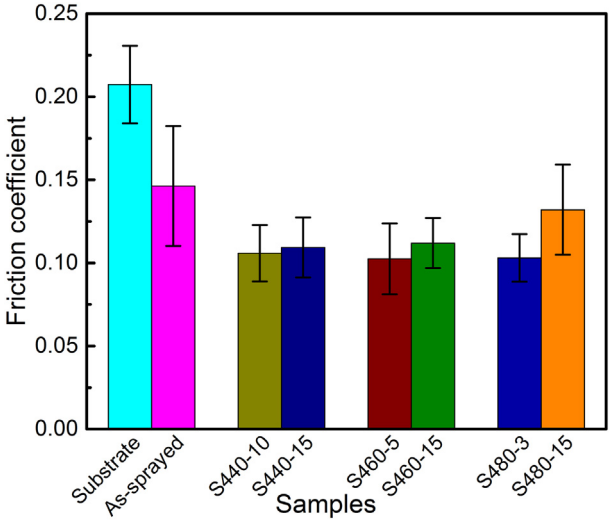

Fig. 2. The friction coefficients of the 2Cr13 steel substrate, the as-sprayed sample, S440-10, S440-15, S460-5, S460-15, S480-3 and S480-15.

treated samples, except for S480-15. S460-5 and S480-3 have the lowest friction coefficients (0.102 and 0.103, respectively). The friction coefficients of S440-15 (0.109) and S460-15 (0.112) are slightly higher than those of S440-10 (0.106) and S460-5 (0.102), which have the highest hardness among the coating samples heated at 440 °C or 460 °C. The friction coefficient of S480-15 (0.132) is about 28% higher than that of S480-3 (0.103). The variations in friction coefficients of samples coincide with the variations in their hardness (Fig. 1). This result indicates that the wear performances of the samples are mainly influenced by their hardness.

Fig. 3 clarifies the average wear volumes of the samples exhibited in Fig. 2. The 2Cr13 steel substrate has the maximum wear volume of 2.063 mm^3, 61% greater than that of the as-sprayed sample (1.281 mm^3). S460-5 and S480-3 have the minimum wear volumes of 0.527 mm^3 and 0.517 mm^3 among the coating samples heated at 460 °C or 480 °C, respectively, almost 60% lower than the as-sprayed sample. After 15-min heat treatment, the wear volumes of S440-15, S460-15 and S480-15 are higher than those of S440-10, S460-5 and S480-3, but still lower than that of the as-sprayed sample. These results are in accordance with the outcomes of the friction coefficient and hardness of

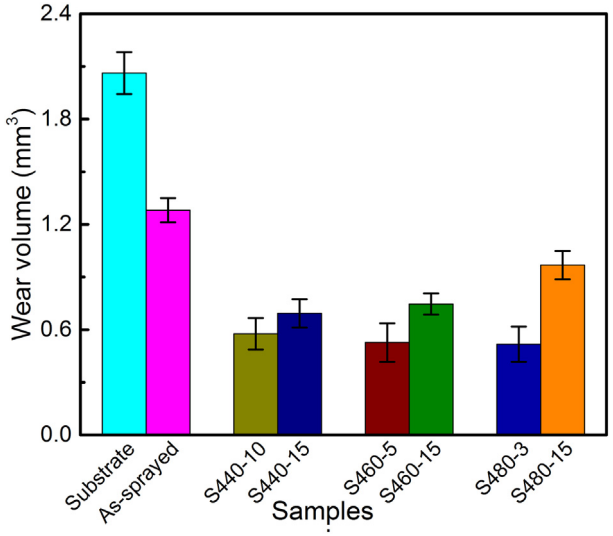

Fig. 3. The average wear volumes of the 2Cr13 steel substrate, the as-sprayed sample, S440-10, S440-15, S460-5, S460-15, S480-3 and S480-15.

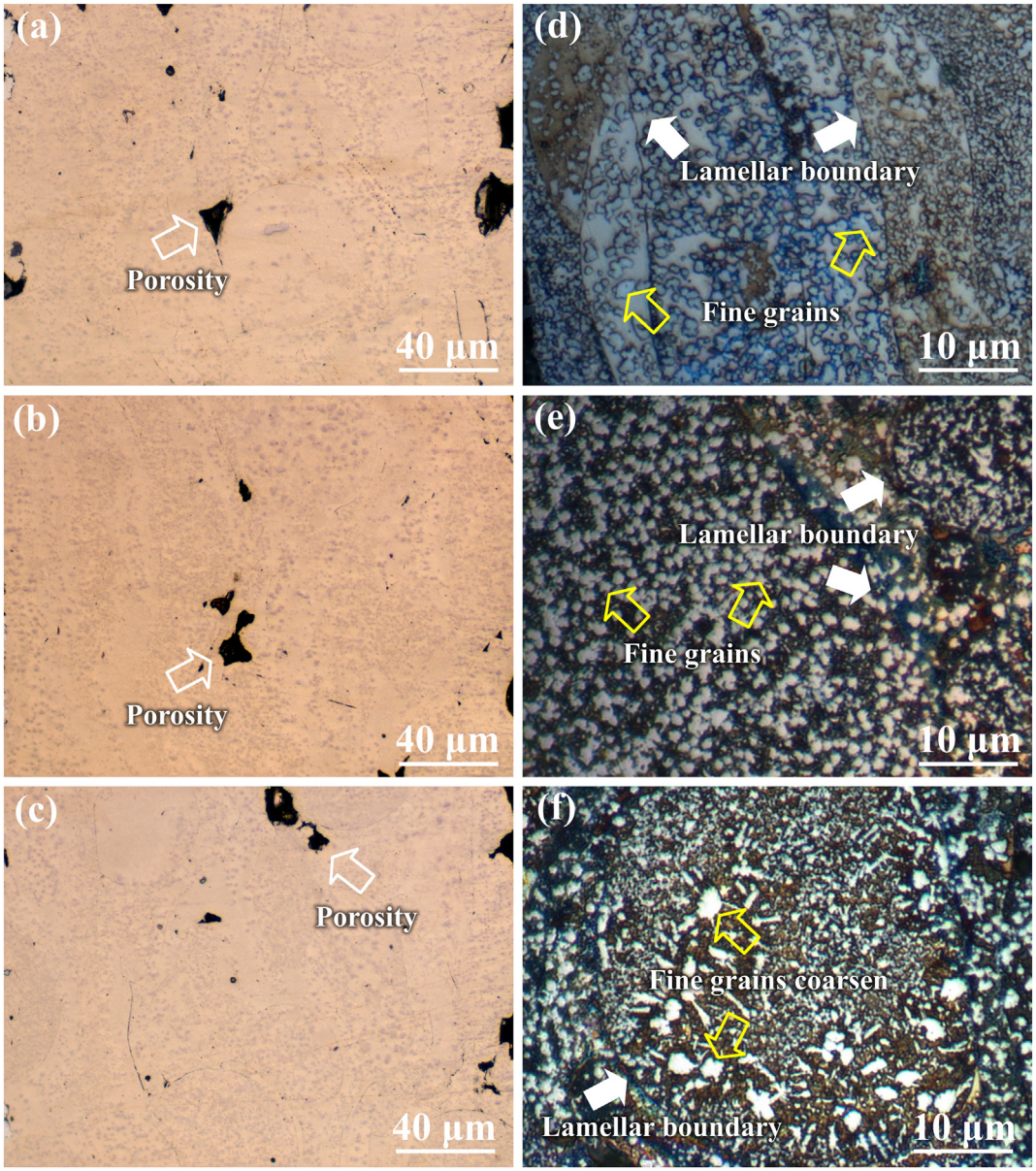

Fig. 4. Metallographic of the non-etched and etched coatings for (a), (d) the as-sprayed sample, (b), (e) S480-3 and (c), (f) S480-15, respectively. The white hollow arrows indicate the porosities in the coatings, the white solid arrows indicate the lamellar boundaries and the yellow triangles indicate the representative fine grains. (For interpretation of the references to color in this figure legend, the reader is referred to the web version of this article.)

these samples (Fig. 2). In general, the samples with lower friction coefficient and higher hardness have lower wear volumes under same testing conditions. Therefore, one can conclude that the short-time heat treatment at the range of 440–480 °C substantially improves both the hardness and the wear resistance of the as-sprayed sample. Because of the prominent improvement in hardness and wear resistance of the coatings after heat treatment at 480 °C, the S480-3 and S480-15 were used for comparison with the as-sprayed sample in the following work.

3.3. Optical microscopy characterization

Fig. 4 shows the OM images of the as-sprayed sample, S480-3 and S480-15. As observed in Fig. 4a–c, pores (as indicated by white hollow arrows) are randomly distributed. The porosity has an important influence on the hardness, and even other properties of coatings [31, 34]. In this work, the average porosities of the as-sprayed sample, S480-3 and S480-15 are 0.75 ± 0.31%, 0.92 ± 0.21%, 0.82 ± 0.28%, respectively, indicating that short-time heat treatment has little influence on the porosities of the coatings. For this reason, the variations in hardness of the coatings should not be associated with the porosity.

Fig. 4d, e and f represents the gradual evolution in microstructures of the as-sprayed sample, S480-3 and S480-15, respectively. Typical lamellar structures of the NiCrBSi coating built up by solidification of molten particles are revealed in the as-sprayed sample, which agrees with the results in the previous reports [20, 35]. The lamellar boundaries are clearly presented as indicated by white solid arrows in Fig. 4d. Fine grains in irregular shape can be found between the lamellar boundaries, which are pointed out by yellow triangles (Fig. 4d). It can be observed that these fine grains are still in submicron-scale. After heat treatment at 480 °C for 3 min, the lamellar boundaries become indistinct and the fine grains (about 1 μm in diameter) are slightly greater than those in the as-sprayed sample (less than 1 μm in diameter) (Fig. 4e). It illustrates that the growth of the fine grains takes place at 480 °C. As heat treatment extends to 15 min, several grains with the size of more than 1 μm are presented in the coating and some lamellar boundaries are almost invisible, as indicated in Fig. 4f. Based on the

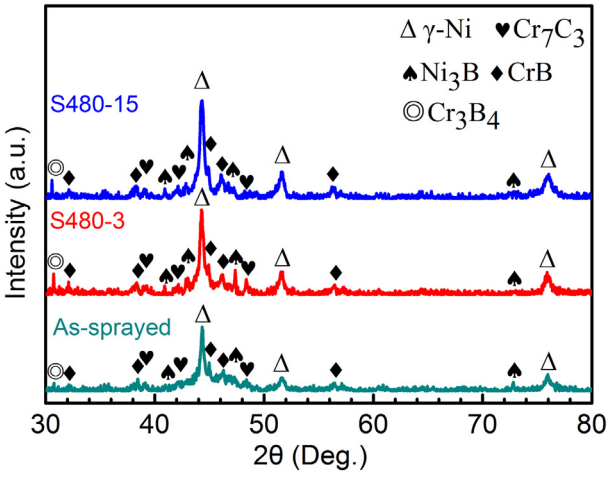

Fig. 5. XRD patterns of the as-sprayed sample, S480-3 and S480-15.

above results, it is clear that the microstructures of the coatings are varied gradually during short-time heat treatment at 480 °C.

3.4. X-ray diffraction

The XRD patterns for the as-sprayed sample, S480-3 and S480-15 are shown in Fig. 5. The phase constituents of the coatings mainly consist of γ-Ni, Ni_3B, Cr_7C_3, CrB and C_4B_3 phases, which are consistent with the results in the literature [15, 20, 36]. No new phase is generated after heat treatment, indicating that the short-time heat treatment does not vary the phase constituents. Compared to the S480-3 and S480-15, the as-sprayed sample is characterized with broadening and lowering peaks. A broad diffuse diffraction maximum is evident at 2θ from 40° to 50°, which is caused by the formation of amorphous phase and/or nanocrystallines [37]. During the spraying process, the NiCrBSi particles are melted or partially melted. It was reported that the time for solidification of these melted or partially melted particles is between about 10^{-8} and 10^{-6} s [23]. Therefore, the amorphous phase inevitably forms in the as-sprayed sample. However, as shown in Fig. 5, the γ-Ni peaks as well as some other peaks (such as the Ni_3B and Cr_3B_4 peaks) become sharper as heat treatment extends, implying that the crystallization of the amorphous phase takes place.

Based on the integrated areas, the volume fractions of all phases detected in XRD are calculated and listed in Table 3. The volume fraction of the amorphous phase decreases monotonously as heat treatment proceeds since the amorphous phase is metastable and it is prone to crystallize at a proper temperature [24, 38]. By contrast, the volume fractions of γ-Ni and Ni_3B increase monotonously from 60.3% to 65.6% and from 4.5% to 8.7%, respectively. The volume fraction of Cr_3B_4 increases after 3-min heat treatment at 480 °C; however, no further augment is observed after 15-min heat treatment. Considering the standard error of XRD, the volume fractions of CrB and Cr_7C_3 keep almost constant. Therefore, once can deduce that the amorphous phase mainly transforms to γ-Ni, Ni_3B and Cr_3B_4, and maybe a trace of CrB and Cr_7C_3.

Table 3
The volume fractions (vol%) of each phase calculated by integrated areas via the XRD patterns in Fig. 5.

Sample	γ-Ni	Ni_3B	CrB	Cr_7C_3	Cr_3B_4	Amorphous phase
As-sprayed	60.3	4.5	16.4	8.5	0.3	10
S480-3	64.3	6.7	16.2	9.7	1.5	1.6
S480-15	65.6	8.7	16.1	8.5	1.1	Undetected

3.5. TEM analyses

The microstructures of the as-sprayed sample, S480-3 and S480-15 were further characterized by TEM as indicated in Fig. 6. Fig. 6a shows that FCC γ-Ni nanocrystallines with the size of about 50 nm are presented in the as-sprayed sample. The halo ring as shown in the corresponding selected area electron diffraction patterns (Fig. 6a inset) elucidates the existence of the amorphous phase in the as-sprayed sample. The TEM-EDS result shows that the amorphous phase contains about 73 ± 3.8% Ni, 14 ± 3.5% Cr, 2.1 ± 0.2% B, 6.6 ± 2.5% Si, 3.7 ± 0.5% Fe and 0.6 ± 0.1% C (in wt%). These values are obtained by five examinations at different amorphous regions. The chemical compositions of the amorphous phase are similar to those of the raw NiCrBSi powder. The fractions of Cr and B decrease slightly, indicating that boride and chromium compounds forms firstly during the progress of deposition. Fig. 6b represents another location in the as-sprayed sample. Dark precipitates with several nanometers indicated by white hollow arrows are resolved as Ni_3B and CrB. In this location, the amorphous phase is also detected (Fig. 6b inset). Therefore, the as-sprayed sample exhibits a mixed microstructure with the amorphous phase and crystalline phase. As heat treatment progresses, more nanocrystallines of γ-Ni are presented in the coating (Fig. 6c). The coarsening grains of γ-Ni are also presented near the nanocrystallines of γ-Ni. The volume fraction of the amorphous phase is reduced and only exists in the gaps of γ-Ni grains as indicated by dash cycle in Fig. 6c. Fig. 6d is another region in S480-3, precipitates surrounded by the amorphous phase are identified as Ni_3B, CrB, Cr_3B_4 and γ-Ni. The size of precipitates seems to be larger than those observed in Fig. 6b, but still in nano-scale. It should be noted that the NiCrBSi coating with this feature has the highest hardness (750 $HV_{0.5}$) and the best wear resistance compared to the as-sprayed sample and S480-15. As seen from Fig. 6e, more coarsening γ-Ni grains are presented and nearly no amorphous phase is observed. Furthermore, coarsening CrB phase with the size more than 500 nm is also observed in S480-15 (Fig. 6f). In terms of the results obtained by TEM analysis, it is easily found that the heat treatment promotes the crystallization of the amorphous phase and the coarsening of grains (such as γ-Ni, Ni_3B and CrB). As mentioned in the Experimental section, the recrystallization temperature of Ni is 417 °C. Hence, the recrystallization of Ni would take place during the heat treatment at all selected temperatures. It is well known that the rates of the crystallization and recrystallization basically depend on the temperature of heat treatment [25]. Therefore, in the case of the lower annealing temperature adopted, a slower increase in the hardness is observed in S440 at the first 10-min heat treatment at 440 °C (Fig. 1). Correspondingly, the slower decrease in the hardness is also found in S440 among the coatings after they reaches the maximum hardness (Fig. 1). For this reason, the decrease in hardness of the coatings after reaching the maximum values should be ascribed to the coarsening of grains.

By combining the XRD results from Fig. 5 and Table 3, it can be confirmed that a large amount of the amorphous phase transforms into crystalline phase at the first 3-min heat treatment at 480 °C. The sizes of the new formed grains embedded in the amorphous phase are within 100 nm. It is speculated that the precipitation of boride and chromium compounds contribute to the increase in hardness and wear resistance of the coatings [39]. As heat treatment proceeds, the amorphous phase is reduced further and the crystalline grains coarsen (Figs. 4 and 6). Both the hardness and wear performance of the coatings confirm again that the rates of crystallization and recrystallization primarily depend on the temperature of heat treatment. If the heat treatment is above the recrystallization temperature of Ni (417 °C), the higher the temperature of heat treatment is, the shorter the time of heat treatment takes to increase the hardness and wear performance (Figs. 1–3). Therefore, after the NiCrBSi coatings reach the maximum hardness and wear resistance, the extended heat treatment above 417 °C would degrade the performance of the NiCrBSi coatings, which also depends on the

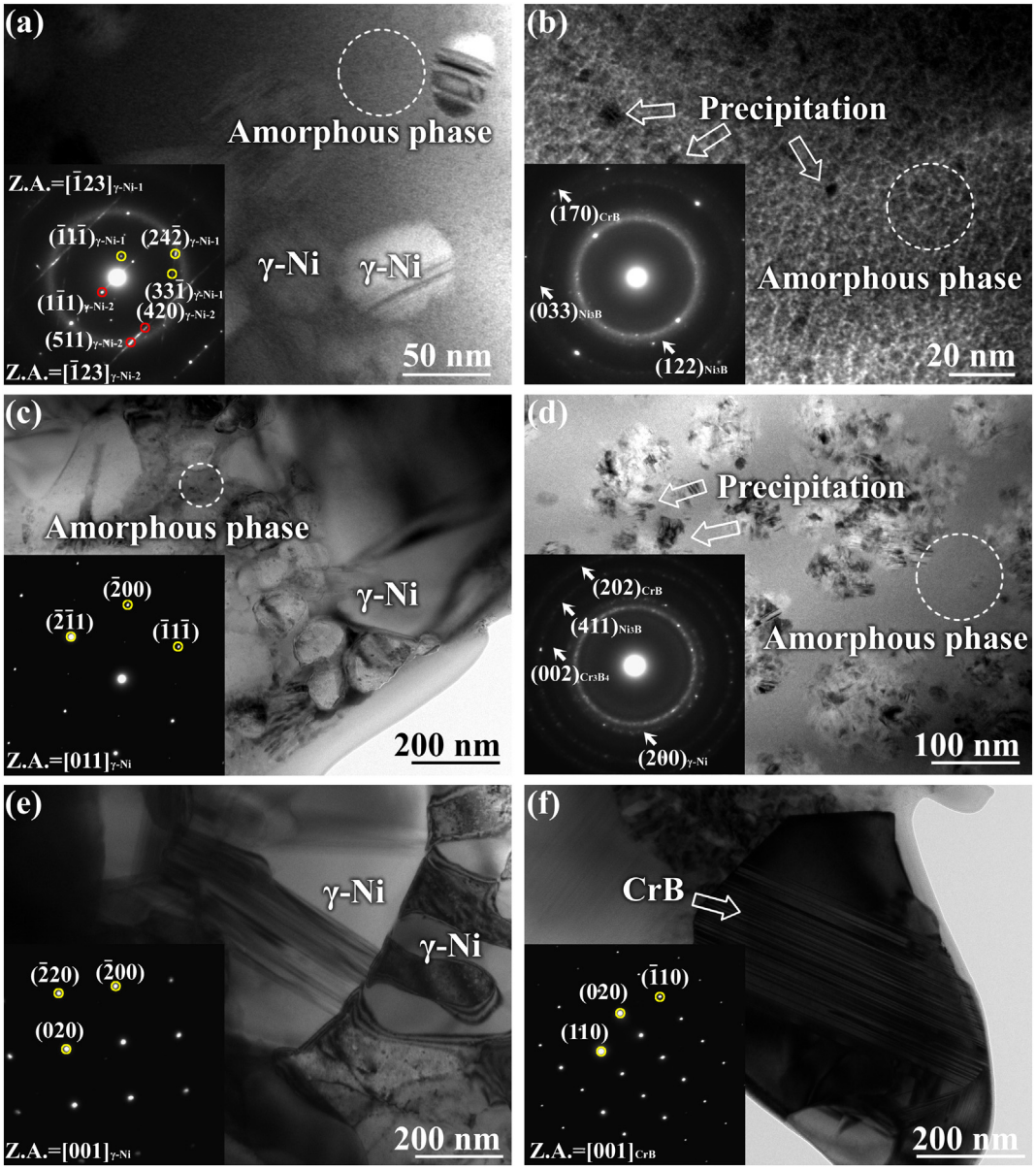

Fig. 6. TEM images of (a), (b) the as-sprayed sample, (c), (d) S480-3, (e) and (f) S480-15. The insets are the selected area electron diffraction patterns corresponding to the amorphous phase, γ-Ni and precipitates in (a)–(f).

annealing temperatures.

3.6. Worn surfaces of coatings

The worn surfaces of the as-sprayed sample, S480-3 and S480-15 examined by SEM are shown in Fig. 7. As seen in Fig. 7a and b, the as-sprayed sample has a very severe abrasive wear phenomenon with some micro-cracks which are caused by stress concentration. Meanwhile, ploughs are formed on the surface of the as-sprayed sample probably due to the abrasive particles provided by the wear debris. The morphology of the wear track of S480-3 is generally smooth with polishing characteristics (Fig. 7c and d). The scratch tracks are shallow and thin (Fig. 7c). Few abrasive wear regions and a small number of micro-cracks distributed on the worn surface are clearly visible (Fig. 7d). Moreover, the slender scratch paralleling to the friction direction is detected. By comparison of the worn surfaces, it can be seen that S480-3 has a higher wear resistance than the as-sprayed sample. The increase in the hardness of the coating would cause the reduction of the contact area between the coating and the friction counterpart, subsequently leading to the less deformation and shear of the coating. For this reason, both the friction coefficient and the wear volume of S480-3 are lower than those of the as-sprayed sample. As seen from Fig. 7e and f, the worn surface of S480-15 is similar to that of the as-sprayed sample. A larger number of abrasive wear regions and micro-cracks are presented on the worn surface of S480-15. Therefore, it can be confirmed that the as-sprayed sample, S480-3 and S480-15 have identical wear mechanism. This should be attributed to the no change in phase constituents of these samples during short-time heat treatment.

3.7. Strengthening mechanism

It is interesting that S480-3 has the highest hardness and best wear resistance among the as-sprayed sample, S480-3 and S480-15. Compared with the phase constituent of the as-sprayed sample, high volume fraction of γ-Ni, Ni_3B and Cr_3B_4 are presented in S480-3 associated with the decline of the amorphous phase (Fig. 5 and Table 3). As is known, for metallic glasses, the crystallization could sharply decrease its toughness, thereby decreasing the strength of alloys [40–42].

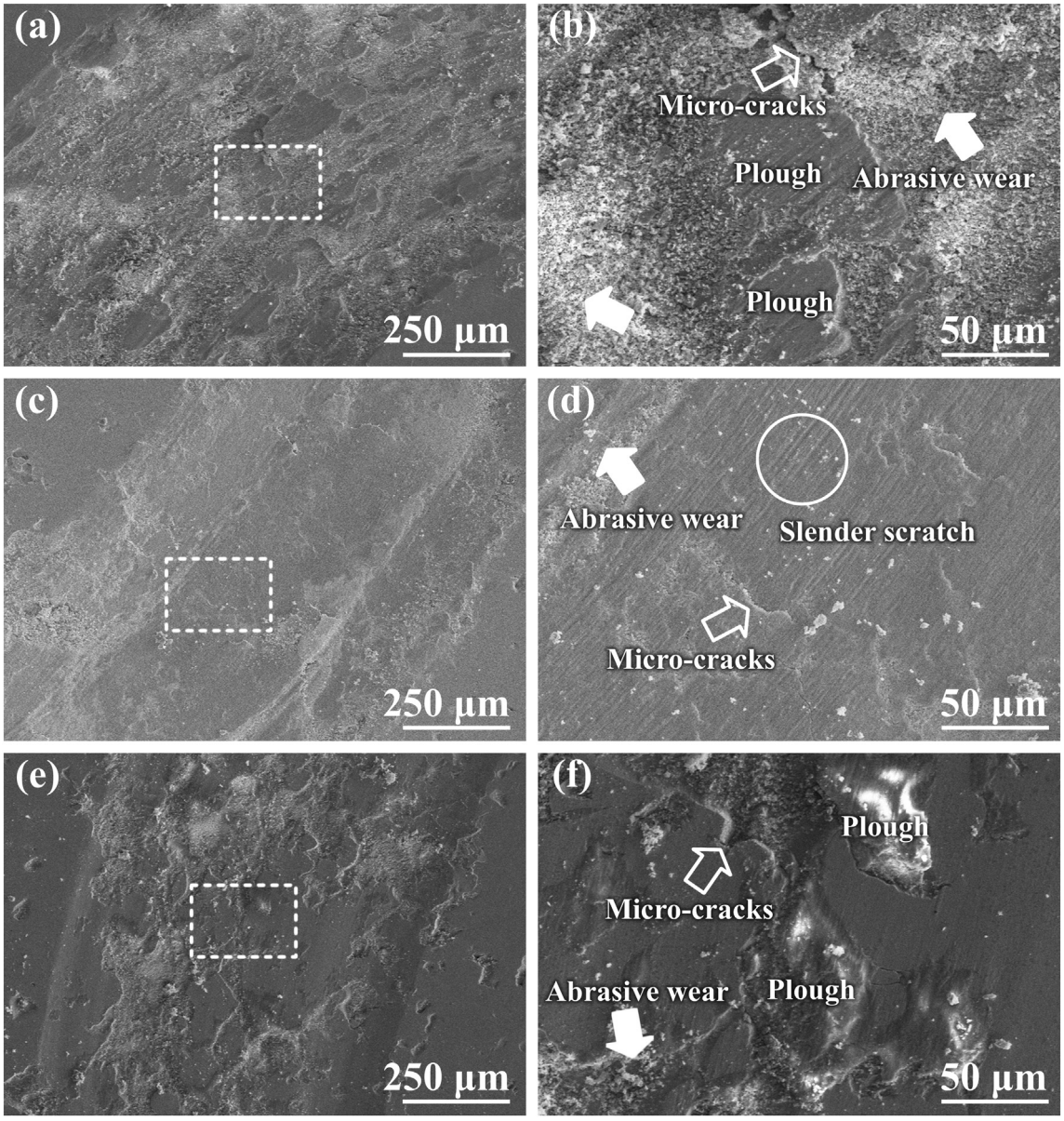

Fig. 7. SEM images for worn surfaces of (a) the as-sprayed sample, (b) S480-3 and (c) S480-15. The (d), (e) and (f) are the magnified images corresponding to the dash rectangles in (a), (b) and (c).

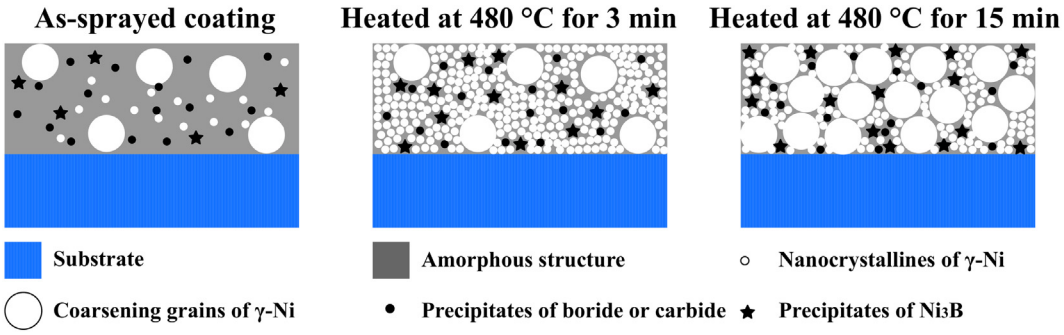

Fig. 8. Schematic illustration for the variation in microstructure of the as-sprayed sample during short-time heat treatment at 480 °C. The amount of amorphous phase, γ-Ni grains and precipitates are only a qualitative representation, not a quantitative representation.

However, when crystallization reaction takes place in the amorphous phase of the as-sprayed sample during short-time heat treatment, boride and chromium compounds precipitates from the amorphous phase. These hard precipitates improve the hardness and wear resistance of the as-sprayed NiCrBSi coating. The similar scenario has been reported by Krishnaveni et al. in electroless Ni–B coating [43]. Furthermore, another strengthening mechanism has been proposed by Wu et al. [44]; a certain amount of nanocrystallines uniformly embedded in the amorphous phase can effectively impede the propagation of main shear bands in the amorphous phase. The alloy with the resultant microstructure can acquire a very high toughness even more than its amorphous phase. In this work, the NiCrBSi coating heat-treated at 480 °C for 3 min results in the partially crystallization of the amorphous phase, which can be described as the uniformly presentation of nanocrystallines embedded in the amorphous region (Fig. 6c and d TEM). Therefore, it may be another reason accounting for the highest hardness and wear resistance for S480-3 among the as-sprayed sample, S480-3 and S480-15.

Based on the discussion above, the evolution in the microstructures of the coatings during heat treatment can be outlined as illustrated schematically in Fig. 8. For the as-sprayed sample, a certain fraction of the amorphous phase (10 vol%) forms in the coating due to the fast cooling rate of melted or semi-melted flight particles during the process of deposition (Table 3). Nanocrystallines of γ-Ni and small particles of hard phases are presented in the amorphous region (Fig. 6a and b TEM). Although the as-sprayed sample has a considerably better hardness and wear resistance properties than the 2Cr13 steel substrate, it still can be further enhanced by short-time heat treatment. Heat treatment provides required activation energy to trigger the crystallization of the amorphous phase in the NiCrBSi coating, thereby leading to the nucleation and growth of the new crystalline phases. As such, more γ-Ni, Ni_3B and Cr_3B_4 are formed after heat-treated at 480 °C for 3 min (Fig. 5 and Table 3). The volume fraction of the amorphous phase is about 1.6% in S480-3. Hence the heat-treated coating is strengthened by the precipitates of hard phases and uniformly distributed nanocrystalline embedded in the amorphous phase as suggested in last paragraph. The NiCrBSi coating with this kind of microstructure has a higher hardness (about 15.4% higher) and a lower wear volume (about 60% less) than the as-sprayed sample. It should be noted that the temperature of the heat treatment plays an important role in increasing the hardness and wear resistance of coating. In this work, the coatings can reach the maximum hardness after heat treatment at all tested temperatures for several minutes. The higher temperature of the heat treatment the faster rate of the crystallization. The maximum hardness of the coating is reached after only 3 min heated at 480 °C. Therefore, this phenomenon is hardly observed if the temperature of heat treatment is too high due to the increased rate of the crystallization and the coarsening of γ-Ni grains. In the previous studies [18–22], the temperature of the heat treatment often approaches the melting point of NiCrBSi alloy or the time of the heat treatment is too long. Hence the NiCrBSi coatings have a coarse microstructure. This is also the result obtained in this study: extended heat treatment leads to coarse grains in the NiCrBSi coating (Fig. 8), thereby degrading its hardness and wear performance. It is difficult to explain which strengthening mechanism is dominant; however, we obtain a NiCrBSi coating with improved hardness and wear resistance. Consequently, it is demonstrated that the short-time heat treatment could improve the hardness and wear performance of the as-sprayed NiCrBSi coating. Although the furnace heat treatment was carried out in the current work, this method might be limited by the furnace size. Since the ideal microstructure has nanocrystalline hard phases that precipitates uniformly and embeds in an amorphous phase, this could be obtained via a few minutes heat treatment at a proper temperature, perhaps by a simple method such as in situ heat treatment by plasma flame of the coating after spraying.

4. Conclusions

In this work, the effects of short-time heat treatment on microstructure, hardness and wear performance of the NiCrBSi coating were systematically investigated. Some key conclusions can be drawn as follows:

(1) The as-sprayed sample has a higher hardness and better wear resistance than the 2Cr13 steel substrate. However, the hardness and wear resistance of the as-sprayed sample could be enhanced by short-time heat treatment at 440–480 °C. The highest hardness of the coatings (750 $HV_{0.5}$) is about 15.4% higher than that of the as-sprayed sample (650 $HV_{0.5}$), and the minimum wear volume of the coating (0.517 mm^3) is about 60% lower than that of the as-sprayed sample (1.281 mm^3). The higher the temperature of heat treatment, the shorter the time for reaching the highest hardness and best wear resistance of NiCrBSi coatings.
(2) The as-sprayed sample possesses a mixed microstructure composed of the crystalline phase and the amorphous phase due to the fast cooling rate of melted and semi-melted flight particles during deposition. After heat treated at 480 °C for 3 min, the volume fractions of Ni_3B, γ-Ni and Cr_3B_4 increase due to the crystallization of the amorphous phase. The precipitates of Ni_3B and Cr_3B_4 are believed to increase the hardness and wear resistance of the coatings. As heat treatment progresses, the γ-Ni grains grow up, leading to a decrease trend of the hardness and wear resistance of the coatings.
(3) The phase constituents of the as-sprayed sample, S480-3 and S480-15 are not varied during the short-time heat treatment as well as the abrasive mode. Therefore, the hardness plays a dominant role in the wear resistance of the coatings. The coating with the higher hardness has the better wear resistance. In the view of the strengthening mechanism, improved hardness and wear resistance of plasma sprayed NiCrBSi coating could be attained via a few minutes heat treatment.

Acknowledgement

The authors would like to acknowledge a financial support provided by National Natural Science Foundation of China (51601075, 51375218 and 51675248), China Postdoctoral Science Foundation Funded Project (2017M611751), and Jiangsu University of Science and Technology Overseas Research & Training Program for University Prominent Young & Middle-aged Teachers.

References

[1] C.W. Chan, S. Lee, G. Smith, G. Sarri, C.H. Ng, A. Sharba, H.C. Man, Enhancement of wear and corrosion resistance of beta titanium alloy by laser gas alloying with nitrogen, Appl. Surf. Sci. 367 (2016) 80–90.
[2] M. Qu, S. Liu, J. He, J. Feng, Y. Yao, X. Ma, L. Hou, X. Liu, Fabrication of recyclable and durable superhydrophobic materials with wear/corrosion-resistance properties from kaolin and polyvinylchloride, Appl. Surf. Sci. 410 (2017) 299–307.
[3] F. Wang, F. Zhang, L. Zheng, H. Zhang, Structure and corrosion properties of Cr coating deposited on, Appl. Surf. Sci. 423 (2017) 695–703.
[4] L. Chai, S. Wang, H. Wu, N. Guo, H. Pan, L. Chen, K.L. Murty, B. Song, α → β transformation characteristics revealed by pulsed laser-induced non-equilibrium microstructures in duplex-phase Zr alloy, Sci. China Technol. Sci. 60 (2017) 1255–1262.
[5] J. Lei, C. Shi, S. Zhou, Z. Gu, L.C. Zhang, Enhanced corrosion and wear resistance properties of carbon fiber reinforced Ni-based composite coating by laser cladding, Surf. Coat. Technol. 334 (2018) 274–285.
[6] P. Yu, L.C. Zhang, W.Y. Zhang, J. Das, K.B. Kim, J. Eckert, Interfacial reaction during the fabrication of $Ni_{60}Nb_{40}$ metallic glass particles-reinforced Al based MMCs, Mater. Sci. Eng. A 444 (2007) 206–213.
[7] S.Y. Chen, G.Z. Ma, H.D. Wang, P.F. He, M. Liu, H.J. Wang, B.S. Xu, Comparison of solidity and fractal dimension of plasma sprayed splat with different spreading morphologies, Appl. Surf. Sci. 409 (2017) 277–284.
[8] L.H. Tian, W. Xiong, C. Liu, S. Lu, M. Fu, Microstructure and wear behavior of atmospheric plasma-sprayed AlCoCrFeNiTi high-entropy alloy coating, J. Mater. Eng. Perform. 25 (2016) 5513–5521.
[9] Y. Wang, G. Cheng, S.L. Tay, Y. Guo, X. Sun, W. Gao, Effects of Bi addition on the

microstructure and mechanical properties of nanocrystalline Ag coatings, Materials 10 (2017) 932.
[10] G. Cheng, X. Sun, Y. Wang, S.L. Tay, W. Gao, Nanoindentation study of electro-deposited Ag thin coating: an inverse calculation of anisotropic elastic-plastic properties, Surf. Coat. Technol. 310 (2017) 43–50.
[11] Z.X. Wang, W.G. Lv, J. Chen, S. Lu, Characterization of ceramic coating on ZK60 magnesium alloy prepared in a dual electrolyte system by micro-arc oxidation, Rare Metals 32 (2013) 459–464.
[12] X. Shi, L. Xu, Q. Wang, L. Xu Sunarso, Hydrothermal sterilization improves initial osteoblast responses on sandpaper-polished titanium, Materials 10 (2017) 812.
[13] B.Y. Zhang, G.J. Yang, C.X. Li, C.J. Li, Non-parabolic isothermal oxidation kinetics of low pressure plasma sprayed MCrAlY bond coat, Appl. Surf. Sci. 406 (2017) 99–109.
[14] F. Arias-González, J. del Val, R. Comesaña, J. Penide, F. Lusquiños, F. Quintero, A. Riveiro, M. Boutinguiza, J. Pou, Fiber laser cladding of nickel-based alloy on cast iron, Appl. Surf. Sci. 374 (2016) 197–205.
[15] S. Dong, B. Song, H. Liao, C. Coddet, Deposition of NiCrBSi coatings by atmospheric plasma spraying and dry-ice blasting: microstructure and wear resistance, Surf. Coat. Technol. 268 (2015) 36–45.
[16] A. Ortiz, A. García, M. Cadenas, M.R. Fernández, J.M. Cuetos, WC particles distribution model in the cross-section of laser cladded NiCrBSi + WC coatings, for different wt% WC, Surf. Coat. Technol. 324 (2017) 298–306.
[17] H.J. Kim, S.Y. Hwang, C.H. Lee, P. Juvanon, Assessment of wear performance of flame sprayed and fused Ni-based coatings, Surf. Coat. Technol. 172 (2003) 262–269.
[18] Z. Bergant, J. Grum, Quality improvement of flame sprayed, heat treated, and Remelted NiCrBSi coatings, J. Therm. Spray Technol. 18 (2009) 380–391.
[19] Z. Bergant, U. Trdan, J. Grum, Effect of high-temperature furnace treatment on the microstructure and corrosion behavior of NiCrBSi flame-sprayed coatings, Corros. Sci. 88 (2014) 372–386.
[20] N. Serres, F. Hlawka, S. Costil, C. Langlade, F. MacHi, Microstructures and mechanical properties of metallic NiCrBSi and composite NiCrBSi-WC layers manufactured via hybrid plasma/laser process, Appl. Surf. Sci. 257 (2011) 5132–5137.
[21] Š. Houdková, E. Smazalová, M. Vostřák, J. Schubert, Properties of NiCrBSi coating, as sprayed and remelted by different technologies, Surf. Coat. Technol. 253 (2014) 14–26.
[22] J. Liu, R. Bolot, S. Costil, M.P. Planche, Transient thermal and mechanical analysis of NiCrBSi coatings manufactured by hybrid plasma spray process with in-situ laser remelting, Surf. Coat. Technol. 292 (2016) 132–143.
[23] H. Singh, B.S. Sidhu, D. Puri, S. Prakash, Use of plasma spray technology for deposition of high temperature oxidation/corrosion resistant coatings - a review, Mater. Corros. 58 (2007) 92–102.
[24] L. Liu, H. Xu, J. Xiao, X. Wei, G. Zhang, C. Zhang, Effect of heat treatment on structure and property evolutions of atmospheric plasma sprayed NiCrBSi coatings, Surf. Coat. Technol. 325 (2017) 548–554.
[25] C.J. Li, Y.Y. Wang, H. Li, Effect of nano-crystallization of high velocity oxy-fuel-sprayed amorphous NiCrBSi alloy on properties of the coatings, J. Vac. Sci. Technol. 22 (2004) 2000–2004.
[26] Z. Jia, X. Duan, P. Qin, W. Zhang, W. Wang, C. Yang, H. Sun, S. Wang, L.C. Zhang, Disordered atomic packing structure of metallic glass: toward ultrafast hydroxyl radicals production rate and strong electron transfer ability in catalytic performance, Adv. Funct. Mater. 27 (2017) 1702258.
[27] L.C. Zhang, K.B. Kim, P. Yu, W.Y. Zhang, U. Kunz, J. Eckert, Amorphization in mechanically alloyed (Ti, Zr, Nb)-(Cu, Ni)-Al equiatomic alloys, J. Alloys Compd. 428 (2007) 157–163.
[28] L.C. Zhang, Z.Q. Shen, J. Xu, Mechanically milling-induced amorphization in Sn-containing Ti-based multicomponent alloy systems, Mater. Sci. Eng. A 394 (2005) 204–209.
[29] N.E. Bacha, Characterization of amorphous plasma sprayed coatings of FeCrPC and NiCrBSi, J. Metastable Nanocrystalline Mater. 18 (2003) 1–8.
[30] A.H. Pakseresht, M.R. Rahimipour, M.R. Vaezi, M. Salehi, Effect of heat treatment on the microstructure and dielectric properties of plasma-sprayed barium titanate films, Int. J. Mater. Res. 107 (2016) 28–34.
[31] ASTM E2109-01(2014), Standard Test Methods for Determining Area Percentage Porosity in Thermal Sprayed Coatings, ASTM International, West Conshohocken, PA, 2014www.astm.org.
[32] S. Ehtemam-Haghighi, Y. Liu, G. Cao, L.C. Zhang, Phase transition, microstructural evolution and mechanical properties of Ti-Nb-Fe alloys induced by Fe addition, Mater. Des. 97 (2016) 279–286.
[33] S. Ehtemam-Haghighi, Y. Liu, G. Cao, L.C. Zhang, Influence of Nb on the $\beta \rightarrow \alpha''$ martensitic phase transformation and properties of the newly designed Ti-Fe-Nb alloys, Mater. Sci. Eng. C 60 (2016) 503–510.
[34] S. Li, Z. Guo, J. Xiong, Y. Lei, Y. Li, J. Tang, J. Liu, J. Ye, Corrosion behavior of HVOF sprayed hard face coatings in alkaline-sulfide solution, Appl. Surf. Sci. 416 (2017) 69–77.
[35] P. Niranatlumpong, H. Koiprasert, The effect of Mo content in plasma-sprayed Mo-NiCrBSi coating on the tribological behavior, Surf. Coat. Technol. 205 (2010) 483–489.
[36] S. Shang, D. Wellburn, Y.Z. Sun, S.Y. Wang, J. Cheng, J. Liang, C.S. Liu, Laser beam profile modulation for microstructure control in laser cladding of an NiCrBSi alloy, Surf. Coat. Technol. 248 (2014) 46–53.
[37] L.C. Zhang, Z.Q. Shen, J. Xu, Glass formation in a (Ti,Zr,Hf)-(Cu,Ni,Ag)-Al high-order alloy system by mechanical alloying, J. Mater. Res. 18 (2003) 2141–2149.
[38] P. Niranatlumpong, H. Koiprasert, Phase transformation of NiCrBSi-WC and NiBSi-WC arc sprayed coatings, Surf. Coat. Technol. 206 (2011) 440–445.
[39] X.C. Zhang, B.S. Xu, Y.X. Wu, F.Z. Xuan, S.T. Tu, Porosity, mechanical properties, residual stresses of supersonic plasma-sprayed Ni-based alloy coatings prepared at different powder feed rates, Appl. Surf. Sci. 254 (2008) 3879–3889.
[40] L.C. Zhang, J. Xu, Glass-forming ability of melt-spun multicomponent (Ti, Zr, Hf)-(Cu, Ni, Co)-Al alloys with equiatomic substitution, J. Non-Cryst. Solids 347 (2004) 166–172.
[41] D.C. Hofmann, J.Y. Suh, A. Wiest, G. Duan, M.L. Lind, M.D. Demetriou, W.L. Johnson, Designing metallic glass matrix composites with high toughness and tensile ductility, Nature 451 (2008) 1085–1089.
[42] N. Nagendra, U. Ramamurty, T.T. Goh, Y. Li, Effect of crystallinity on the impact toughness of a La-based bulk metallic glass, Acta Mater. 48 (2000) 2603–2615.
[43] K. Krishnaveni, T.S.N.S. Narayanan, S.K. Seshadri, Electroless Ni-B coatings: preparation and evaluation of hardness and wear resistance, Surf. Coat. Technol. 190 (2005) 115–121.
[44] G. Wu, K.C. Chan, L. Zhu, L. Sun, J. Lu, Dual-phase nanostructuring as a route to high-strength magnesium alloys, Nature 545 (2017) 80–83.